Applied Energy 183 (2016) 133–147

Contents lists available at ScienceDirect

Applied Energy

journal homepage: www.elsevier.com/locate/apenergy

Evaluating solar irradiance over facades in high building cities, based on LiDAR technology

A. Martínez-Rubio [a], F. Sanz-Adan [b,*], J. Santamaría-Peña [b], Araceli Martínez [c]

[a] ARESOL Renewable Energies Group, Spain
[b] University of La Rioja, Spain
[c] SAITEC Bilbao, Spain

HIGHLIGHTS

- A method for evaluating solar irradiance over façades in building cities with mutual shading.
- It calculates irradiance curves in all building façades, using LiDAR and irradiance information.
- Solar irradiation maps of the city buildings are really important for urban planning.
- It allows to selection BIPV elements depending of the irradiation in each façade point.
- The model can be extrapolated to all the building envelope.

ARTICLE INFO

Article history:
Received 10 March 2016
Received in revised form 26 August 2016
Accepted 27 August 2016

Keywords:
BIPV
LiDAR
Shading facades
Solar irradiance

ABSTRACT

Arranging a solar irradiation map of the buildings of a city is a valuable tool for sustainable urban planning in regard to non-carbonized criteria in important applications. Such applications may include: selection of materials for the building envelope and insulation according to the irradiation received at each point; monitoring the installation of photovoltaic systems to ensure that they are located in the optimal irradiance zones; or building restoration to improve the energy efficiency and electric generation.

The proposed method enables to estimate the incidence of the solar irradiance as well as to visualize the effect it produces in every region of the buildings that compose the urban area of a city. The process includes the use of Laser Imaging Detection and Ranging (LiDAR) information along with 5-min horizontal irradiance data. This developed algorithm has been verified through being applied to different building envelopes distributed in different geographical areas. The results demonstrate a satisfied performance which makes that the methodology can be extrapolated to any city where the LiDAR Data and irradiance information are available, permitting an accurate analysis of the solar irradiance over the building envelopes.

The algorithm succeeds in obtaining a map of solar radiation captured by the envelope of any urban building that estimates the photovoltaic power generation depending on the geographic location and on the influence of shading caused by adjacent buildings. The provided results show clear evidence of the influence of the shade effect produced by both, the building itself and other nearby buildings. Even if the shading effect is a factor that determines the irradiation gradient, the orientation of the facades has been proven to be the most important parameter in seeking a higher value of irradiation. As a result, south facing walls present wider regions with greater irradiance values, which are of interest for photovoltaic implementation. In addition, monthly analyses have shown that the best-oriented facades have produce their maximum solar power during equinox months, March and September.

This method is considered as a useful tool for sustainable urban planning and for building integrated photovoltaics development. Although the entire envelope of a building can be studied, this paper is limited to the analysis of the facades.

1. Introduction

Combating climate change through a decarbonized economy is a priority of the Europe 2020 strategy [1]. The importance and

* Corresponding author.
E-mail addresses: albertomartinezrubio@hotmail.es (A. Martínez-Rubio), felix.sanz@unirioja.es (F. Sanz-Adan), jacinto.santamaria@unirioja.es (J. Santamaría-Peña), aracelimartinezrubio@gmail.com (A. Martínez).

http://dx.doi.org/10.1016/j.apenergy.2016.08.163
0306-2619/

potential of solar photovoltaic energy to achieve this objective is unquestionable. Currently, solar photovoltaic technology, despite its low efficiency (between 10 and 20%, depending on the type of technology [2–4]), can reach grid parity in certain geographic areas [4]. So far, the existing implementation of photovoltaic generators in buildings is accomplished mainly by means of elements added to the roofs of buildings or by the construction of attached photovoltaics (BAPV), which provide a questionable aesthetic solution.

Over last decade, building integrated photovoltaics (BIPV) products of various efficiencies have been developed in the solar sector in order to improve urban integration [4].

The evolution of photovoltaic technology allows to establish that depending on the technology and BIPV solutions applied to roofs [5,6] or facades [5,7,8] costs have been reduced as the efficiency values have gone up. There are multiple BIPV products that can be implemented in every building and situation: claddings with different azimuth angles [9], facade shading elements (carport, awning, shutter and eaves) [10], windows with semi-transparent solar cells [11], skylights and atriums [12,13].

The mentioned solutions have already been implemented in pilot buildings throughout the world, presenting problems of its multiplying effect as a consequence of an inaccurate previous study of the solar resource, its incidence over the different faces and an incorrect placement of PV elements on the building envelope [14–18].

There are various prestigious databases that enable one to predict the solar irradiation received in a specific geographical location, given its coordinates and altitude, as well as the orientation of the plane (azimuth and zenith) and its tracking system (fixed, horizontal, vertical or polar axis) [19,20].

Allowing the analysis of the solar irradiance received by the buildings, several algorithms which are based on the data supplied by local weather stations or on the already mentioned databases, have been developed and published. The provided results allow to optimize the position and orientation of the photovoltaic elements (BAPV and BIPV), to determine the annual efficiency and to obtain the output energy; fundamental factors that define the internal rate of return and the pay back of the photovoltaic investment [21–23]. Marked improvements are introduced when the shading of nearby buildings and obstacles on roof-top photovoltaic systems is calculated [24,25].

While Laser Imaging Detection and Ranging (LiDAR) technology enables one to obtain an initial approximation of the energy resource of urban building's roof-tops, there are other algorithms that permit the detection of production losses as consequence of the fact of setting obstacles on roofs top, such as fireplaces, caissons or antennas. One can conclude that most of the roofs of the buildings are uneconomic from an energy point of view. Thus, one must determine which areas are suitable for photovoltaic implementation [26–28].

The presented research enables to obtain the annual average solar irradiance at every point of the facades of the buildings in a city by the use of LiDAR technology, taking into account the shading effect produced by nearby obstacles and buildings. The result is an algorithm that, using the data obtained from a LiDAR flight over any city, determines the solar irradiation curves of the facades of every building, allowing one to determine the solar energy potential of the different areas of a building.

The solar energy potential of a building in an urban environment is defined by the location of well-positioned planes in the roof-top and facades. Several authors have already studied different methodologies for the purpose of identifying the buildings in large cities, converting them into three-dimensionally triangle surfaces by means of available classified LiDAR data [29–31]. The process that was developed by [29] is used in this paper.

The photovoltaic potential of the different facades of buildings is defined by the specific exposure to sun rays. While in the case of analyzing the roofs photovoltaic potential, their orientation and inclination must be determined, in the case of facades (which are by definition vertical planes), the factors to be considered are their orientation and any shading effect produced by other planes o f facades or nearby buildings.

In order to study the incidence of the solar irradiation over each surface, the algorithm converts the triangles into grid points. Taking account for all the potential obstacles such as shadings, the global computation of incident solar irradiation at every point of a facade generates iso-irradiance curves, which are called solar irradiance curves in this paper. The proposed methodology classifies the building envelopes and facades according to its irradiance incidence.

The applications that arise from this method include the following:

- Sustainable urban management to project new constructions, the restoration and rehabilitation of buildings, urban renewal, sustainability improvement of cities, the determination of the energy requirements of buildings (cooling and heating) or energy generation potential (heat and electricity).
- Support of architects and engineers in designing the building envelope (new and existing), optimizing the aesthetics/efficiency relationship. This includes BIPV solutions that improve the insulation of the building (materials that will reduce the transmittance) and generate solar energy (improve orientation). These solutions present great opportunities to meet three important objectives: reducing the energy consumption of buildings, increasing energy self-consumption (reducing transportation losses) and regenerating degraded urban areas [32,33].
- Allow promoters and communities to foresee the investment's payback.
- Serve as a valuable tool by which manufacturers of PV systems can improve the market's knowledge of BIPV materials and products, presenting solutions that are both economically and technologically feasible to urban planners and developers.

Whereas in the methodology that was described by Gooding et al. [34], a catalogue of common roof shapes are assigned to buildings, the algorithm presented in this paper locates and features geometrically (shape, orientation and slope) both, roofs and facades, according to the actual shape of the LIDAR points defined. Similarly, Tooke et al. [35] use LiDAR information to model the building energy demand for contiguous regions within urban areas. In addition to this, the proposed method enables one to define more accurately the solar irradiation at any point of the building envelope as well as to consider the negative effect of shading.

2. Method

The main purpose of this paper is to propose an algorithm to analyze the incident irradiation on building facades in large cities, by the use of LiDAR (Laser Imaging Detection and Ranging) information and monthly irradiance data. The algorithm has been developed using VisualBasic©. As can be seen in Fig. 1, the method

Fig. 1. General methodology.

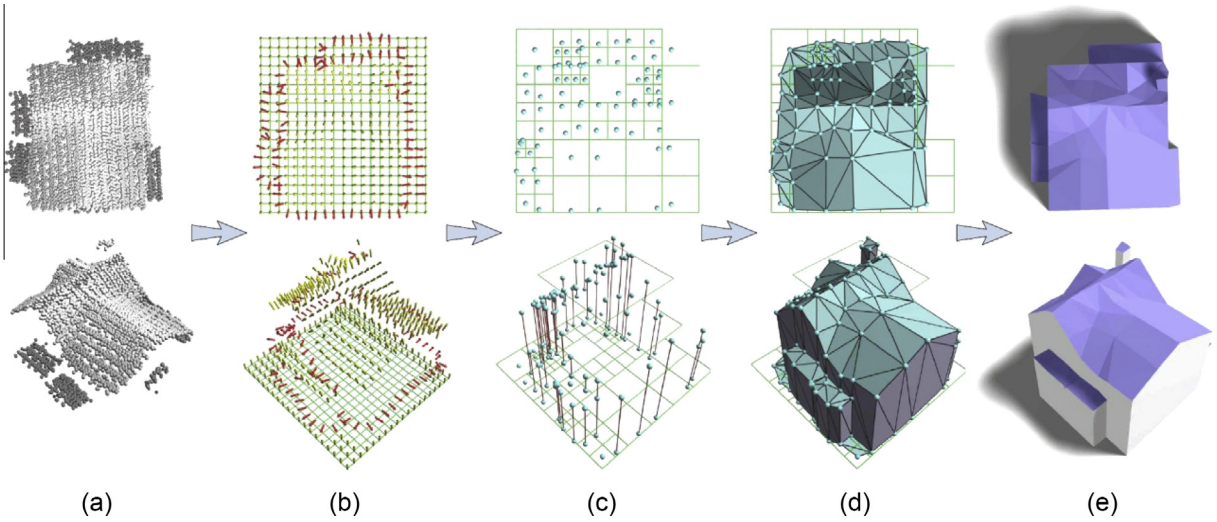

Fig. 2. Methodology used to obtain the triangulation of buildings from LIDAR data [29].

contains five steps: modeling, discretization, shading effect study, irradiance model application and presentation of the results.

2.1. Building 3D modeling from LiDAR data

The proposed method starts with the modeling, which permits the triangulation of the different constructions that are located in the study area. The input is the filtered and classified LiDAR data. Thus, a three-dimensional cloud of points may serve as a base to generate surfaces that are built with triangles.

There are different methods to obtain digital models of buildings from LiDAR data, and the one proposed by Zhou [29] has been selected. It is remarkable that the modeling part has been limited to the verification of the building construction done by Zhou's software. A filter is applied in order to consider ground and building points of the LiDAR information. Thus, other elements, such as trees, are not considered in this paper.

For easier understanding, the building modeling by Zhou [29] is divided into four parts:

1°. Scan conversion - The point cloud is embedded in a uniform 2D grid. Surface Hermite data samples (gold arrows) are generated at grid points and boundary Hermite data samples (red[1] arrows) are estimated on grid edges that connect different roof layers (see Fig. 2b).
2°. Adaptive creation of geometry - A hyper-point is computed in each quadtree cell by minimizing a 2.5D QEF (quadratic error function). Geometry simplification is achieved in an adaptive manner by collapsing subtrees and adding QEFs that are associated with leaf cells (see Fig. 2c).
3°. Polygon generation- A watertight mesh model is reconstructed by connecting hyper-points with surface polygons (turquoise triangles) and boundary polygons (purple triangles), which form building roofs and vertical walls, respectively (see Fig. 2d).
4°. Principal direction snapping - The roof boundaries are refined to follow the principal directions (see Fig. 2e).

It must be noted that the calculation of incident irradiance has only been applied to facades, although there is an opportunity to increase its application to the entire building envelope. In any event, the first step consists on creating surfaces that are constructed by triangles that represent the complete buildings' envelopes.

2.2. Discretization

Once the model has been constructed with triangles, it is necessary to study the incidence of annual solar irradiance acting on each triangle. Instead of analyzing the behavior of the entire triangle, this research aims to generate test-points, which are used as representative points of the triangle during shading and irradiance studies. If the discretization has enough resolution, the results will surely be accurate.

This process requires less time to calculate the shading effect of the model than do other methods, such as polygon intersection. This time reduction is due to the fact of using simpler algorithms where the goal is to determine if a test point is inside a triangle.

The test-point generation is defined by a system of relative coordinates that consider – for the plane formed by the triangle - the X axis as the direction resulting from the intersection of the triangle's plane and the horizontal plane, the Y axis as the direction of the maximum slope of the triangle's plane and the Z axis as the normal direction of the triangle's plane. Test-points of each triangle are then generated by creating a determined and modifiable 0.5 m size grid, which is of higher resolution than the grid of 1 m resolution that was used in [28].

In Fig. 3, an example of the discretization can be seen, in addition to a graphic explanation of the grid development that was previously mentioned.

2.3. Shading study

As it can be seen in Fig. 1, the shading study is the third part of the proposed algorithm. The solar position is calculated by means of the solar declination angle that was proposed by Cooper [36]. Each test-point generated during the previous step is then analyzed to determine the possible shading effect influence produced by a triangle of the model.

As shown in Fig. 4, the test-points are projected to the obstacle triangles along the solar vector direction. Finally, a shading map of the points for each sun position in which the points may be presented in two different conditions (shaded or un-shaded) is obtained. Each shading map is unique and is dependent of the solar vector direction. Thus, the time at which the solar position changes the shading map must be updated.

[1] For interpretation of color in Figs. 2 and 14, the reader is referred to the web version of this article.

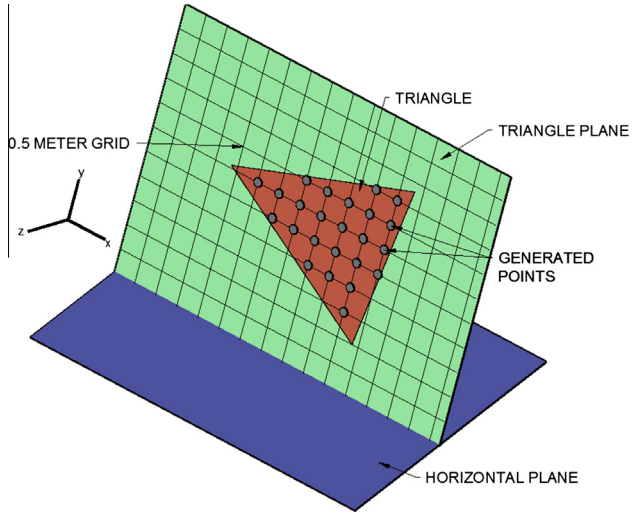

Fig. 3. Discretization of the triangle.

Considering that the model may be formed by thousands of elements, some routines have been added in order to reduce the calculation time. The most important one implies that, once a test-point has been determined to be as shaded by a triangle, nearby triangles are studied to determine the shading of each test-point by the triangle to which it belongs. Other noticeable improvement consists on calculating the angle of incidence between the solar vector and the normal vector of the test-point triangle's plane, so when it exceeds 90°, it implies that every test-point that the triangle contains is shaded.

2.4. Irradiance model

The irradiance model of Perez et al. [37] is considered to be the baseline, but has been modified to be adapted to an urban environment. The model proposed by Perez et al. [37] considers the effect of direct irradiation from the sun (beam), as well as other sources like clouds, sky dome or the horizon (diffuse), and it is used to evaluate the irradiance on sloped surfaces. As can be seen in Fig. 5, it presents five irradiance terms: the beam, circumsolar diffuse, isotropic diffuse from sky dome, diffuse from the horizon and ground-reflected irradiation.

In order to provide a more reliable model that is suitable for the urban environment, the diffuse radiation from the horizon and ground-reflected irradiance has been exchanged for the diffuse irradiance that is reflected by the nearby buildings' envelopes. As shown in Fig. 5, the solar irradiance that affects the nearby buildings is evaluated by separating those areas that are partially shaded from those that have direct irradiance influence. The solar irradiation is then reflected as diffuse irradiation that potentially affects the studied point. It must be noted that the influence of reflecting facades is not considered in other proposed methods, such as [28].

The effect of shading by nearby buildings' envelopes needs to be evaluated. The methodology that was previously explained is used (parts 2 and 3 of the proposed method that appears in Fig. 1).

The isotropic diffuse is the irradiance that comes from the sky dome and in the original Perez et al. model [37] is limited by the irradiance level and the inclination of the plane. This research makes a reduction in the visible sky dome area by means of the horizon profile accounting for the effect of shading created by nearby buildings, as shown in Fig. 6. A few examples are presented in the application part for better understanding.

Eq. (1) represents the Perez et al. [37] irradiance model after having been adapted to an urban environment:

$$\begin{aligned} G_{global} = {} & G_{bh} \cdot \frac{\cos(\theta)}{\cos(\theta_h)} \cdot sh + G_{dh} \cdot F_1 \cdot \frac{a}{b} \\ & + G_{dh} \cdot (1 - F_1) \cdot \left(\frac{1 + \cos(\beta)}{2}\right) \cdot vis \\ & + \sum_{i=1}^{n1} \left[G_{inc,unshaded} \cdot \left(\frac{1 + \cos(\alpha)}{2}\right) \cdot \rho \right] \\ & + \sum_{i=1}^{n2} \left[G_{inc,shaded} \cdot \left(\frac{1 + \cos(\alpha)}{2}\right) \cdot \rho \right] \end{aligned} \quad (1)$$

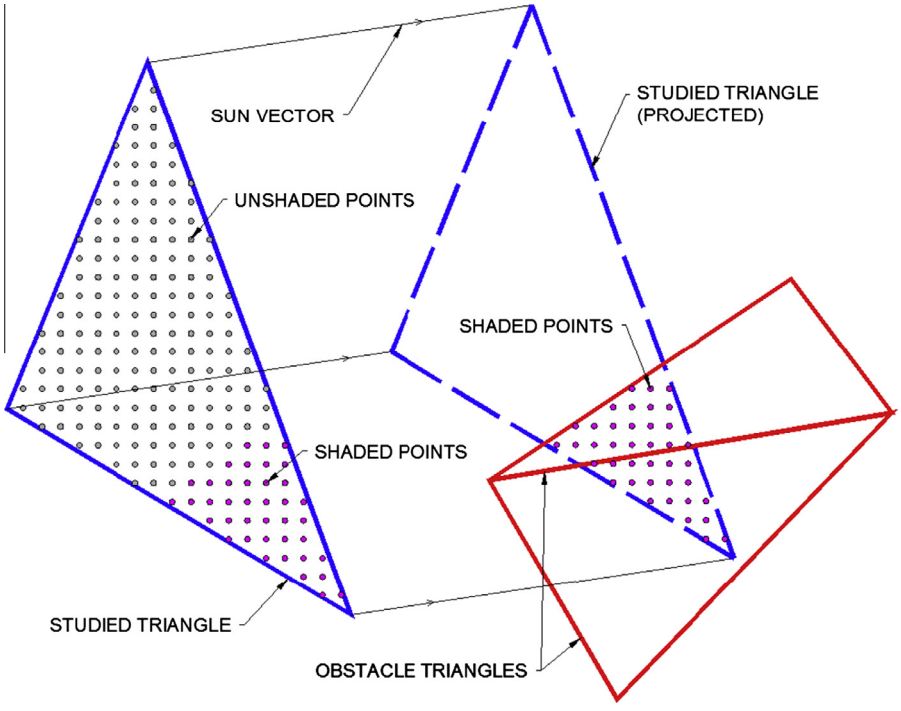

Fig. 4. Test-point shading analysis.

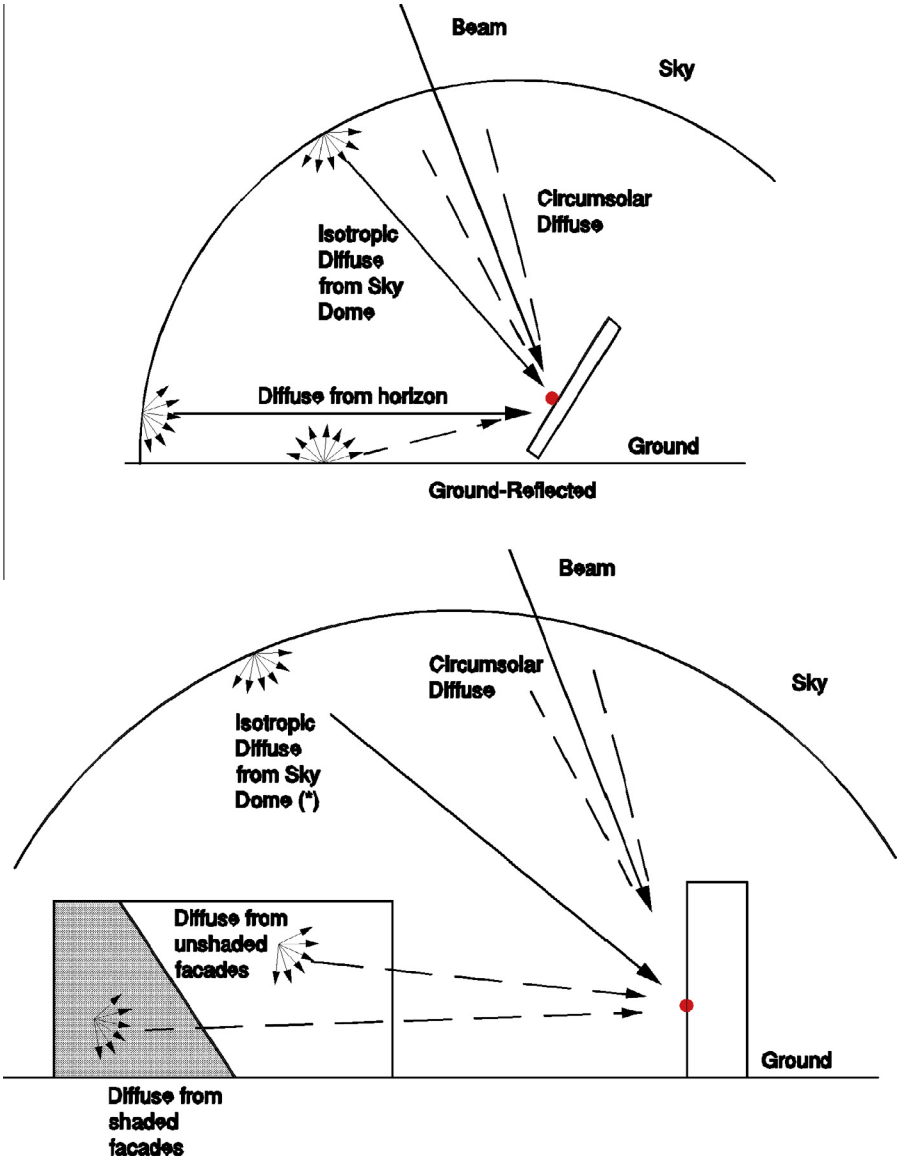

Fig. 5. Adaptation (a) of Perez irradiance model to an urban environment (b).

where G_{global} is the total irradiance incident over the test-point (W/m^2), G_{bh} is the horizontal beam irradiance term (W/m^2), θ is the incidence angle (°), θ_h is the solar zenith angle (°), sh is the shading effect (0 or 1), G_{dh} is the horizontal diffuse irradiance term (W/m^2), F_1 is the circumsolar brightness coefficient, a and b are terms that account for the angles of incidence of the cone of circumsolar radiation, β is the triangle plane inclination (°), vis is the visible sky percentage for the horizon analysis of each test-point (%), $G_{inc,unshaded}$ is the global irradiation over n1 nearby facades that are free of shadows (W/m^2), $G_{inc,shaded}$ is the global irradiation over n2 nearby facades that are shaded (W/m^2), α is the angle between the triangle's plane and the nearby facade (°), and ρ is the reflection term of each nearby facade (%).

2.5. Output data

To conclude the method, series data results are presented in the basis the irradiation is introduced, in this paper 5-min. The results include the global direct and diffuse irradiance values for every test point and temporal series. Additionally, it is possible to differentiate between the different irradiance terms involved in the solar irradiance incidence process, as well as to evaluate the effect of the shading produced by nearby buildings.

In order to obtain the optical losses using the IAM factor concept, the incidence angle is determined so it is applied to the irradiance model, whereas in other papers is not calculated [28]. In addition, an algorithm for graphical interpretation that creates a 3D model of the building and the iso-irradiance curves over the facades in Autocad© has been developed.

2.6. Case study

The model has been applied to an area of Logroño (La Rioja, Spain), a city of 152,000 people that covers an area of 80 km^2 and contains population density of 1900 inhabitants per km^2. This city's geographical coordinates are 42°28′12″ north and 2°26′44″ west.

The LiDAR database used is *Plan Nacional de Ortofotografía Aérea* (PNOA) flights project [38] from the Spanish Government. The objective of this project is to cover all territory of Spain through point clouds obtained by airborne LiDAR sensors, with a density of 0.5 points/m^2. PNOA provides LiDAR information for such

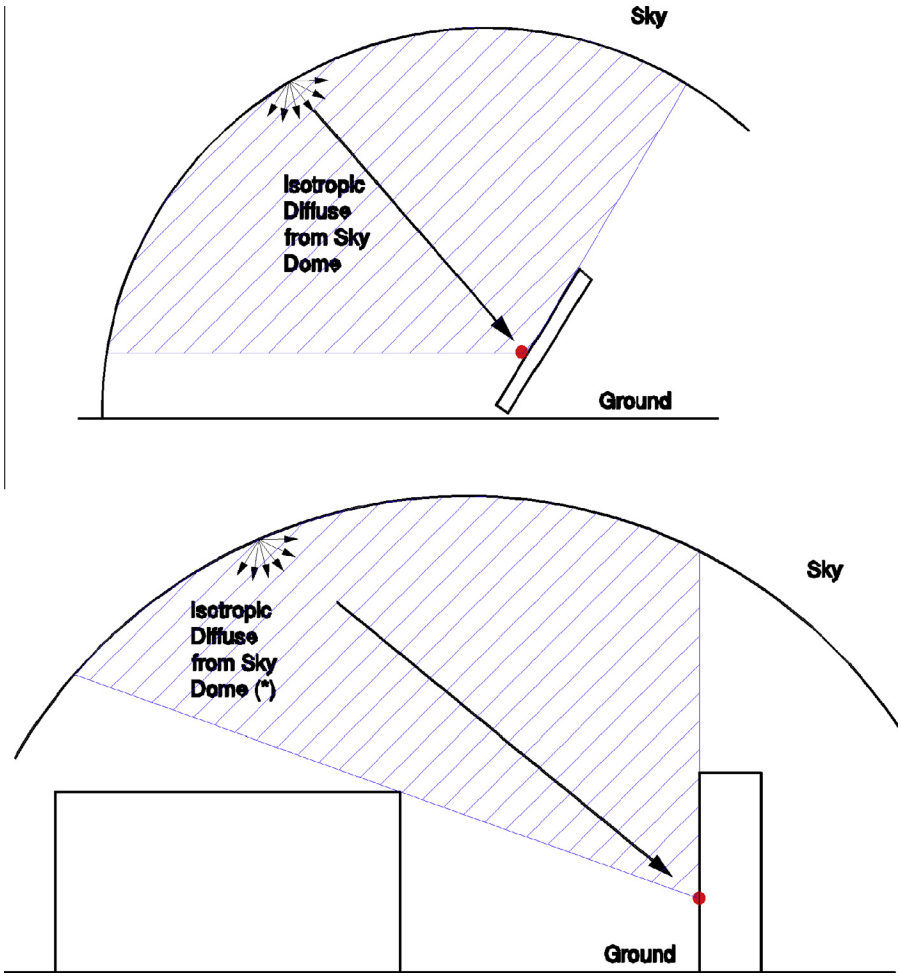

Fig. 6. Visible sky dome for isotropic diffuse irradiation (a) adapted to an urban environment (b).

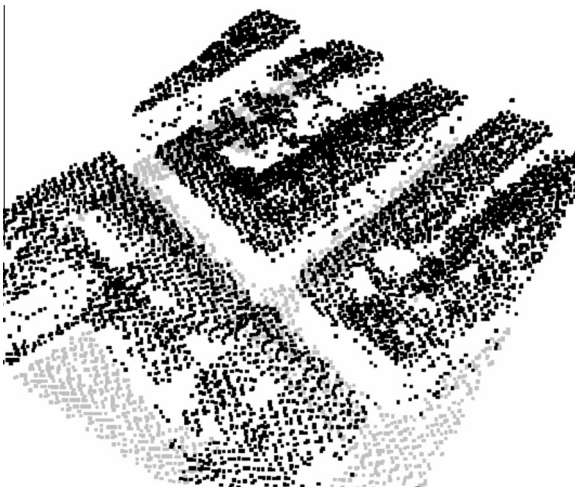

Fig. 7. LIDAR cloud-point data [38].

well-known applications including terrain digital model generation or flooding analysis in rural zones, as well as new ones that are similar to the presented in this paper and which uses the existing information of large cities.

Considering that the aim of a model application is to test the proposed model, the confluence of two streets in the center of Logroño that consists of buildings from 4 to 7 floors and a street width of 14 m has been selected. In Fig. 7, one can see the point cloud that is considered for the model application, on which black-colored points are building points that are differentiated from the gray-colored ground points.

In order to reduce the calculation times and accepting that the results can be extrapolated to any type and number of facades or buildings, just some certain areas of the facades have been selected. In addition, even if the first step of the method was applied to the complete cloud point that is shown in Fig. 7, the rest of the method was applied only to a specific limited area. The selected building has its facades oriented in two main directions as shown in Figs. 8–11. Considering as reference north and a clockwise angle direction, one is 285° for walls number 1 and 5 (West), another 195° for walls number 2, 4 and 6 (south), and another 105° for wall number 3 (east).

The existence of two nearby buildings south and west oriented must be noted in order to check the influence they have in the irradiance capture levels of the facades. The adjacent building that is located to the west is considerable higher, being about 27 m height, while the one that is located to the south is about 17 m height (see details in Fig. 9).

Having considered a 0.5 m grid size, the discretization of triangles involved a total of 8362 test-points. As shown in Figs. 9 and 10, the selected building is divided into a ground floor level that is four meters height (ground floor), and four upper floors, each of which is three meters high (1st floor, 2nd floor, 3rd floor and 4th floor). The algorithm studies the behavior of a series of test-points which, depending on the floor to which they belong, are easy to

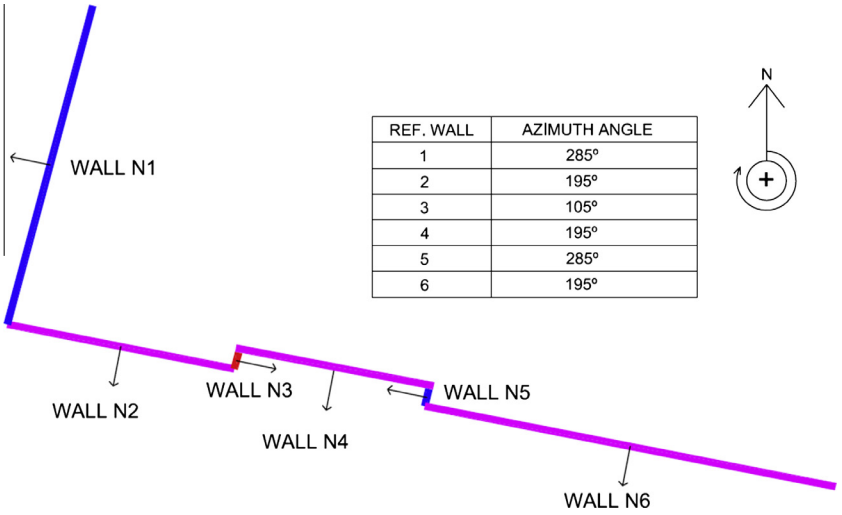

REF. WALL	AZIMUTH ANGLE
1	285°
2	195°
3	105°
4	195°
5	285°
6	195°

Fig. 8. Orientation of Walls.

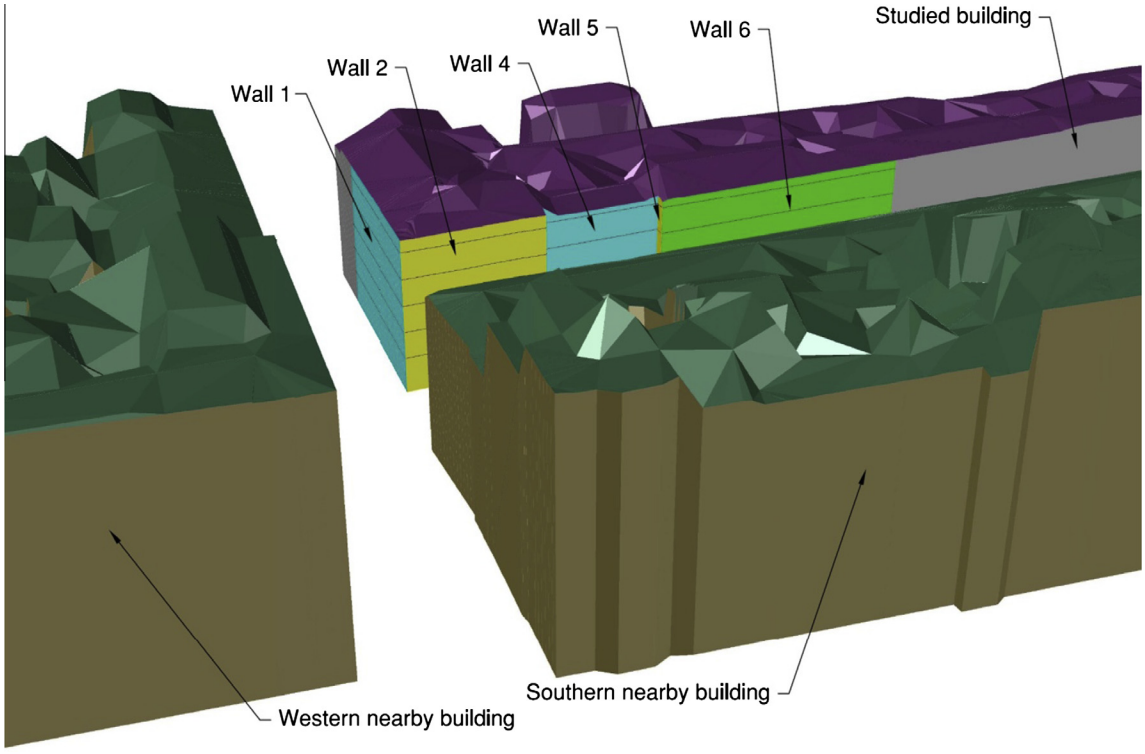

Fig. 9. Triangulation model obtained from LiDAR data (i).

characterize in terms of shading and solar irradiance incidence. Thus, the entire surface performance is perfectly defined. In this case, those points whose elevation (Z) is less than or equal to 4 m belong to the ground floor, up to 7 m the first floor, up to 10 m to the second floor, up to 13 m to the third and finally up to 16 m in height the fourth floor.

Table 1 shows the number of test-points contained in each facade of the building depending on the floor where it is located, in addition to the surface of each of the studied facades. The quantity of test-points is greater in the case of the lowest floor (ground floor) because it is one meter higher than the others.

In order to calculate the visible sky percentage for the irradiance model, as it has been previously explained, every test-point is analyzed regarding the visible sky dome. As shown in Figs. 12 and 13, there are two examples of the horizon profile of two test-points, one is located in wall number 1 and the other in wall number 2. It can be seen that the horizon profile is modified depending on both, the triangle orientation and nearby buildings and obstacles.

Taking account for the monthly irradiation values provided from PVGIS© [39], 5-min basis synthetic series that enable to achieve a correct characterization of the shading effect are generated using Gaussian models [40,41].

2.7. Checking the method

One of the most crucial parts of every proposed method is the validation. In this case, it has been used an experimental research

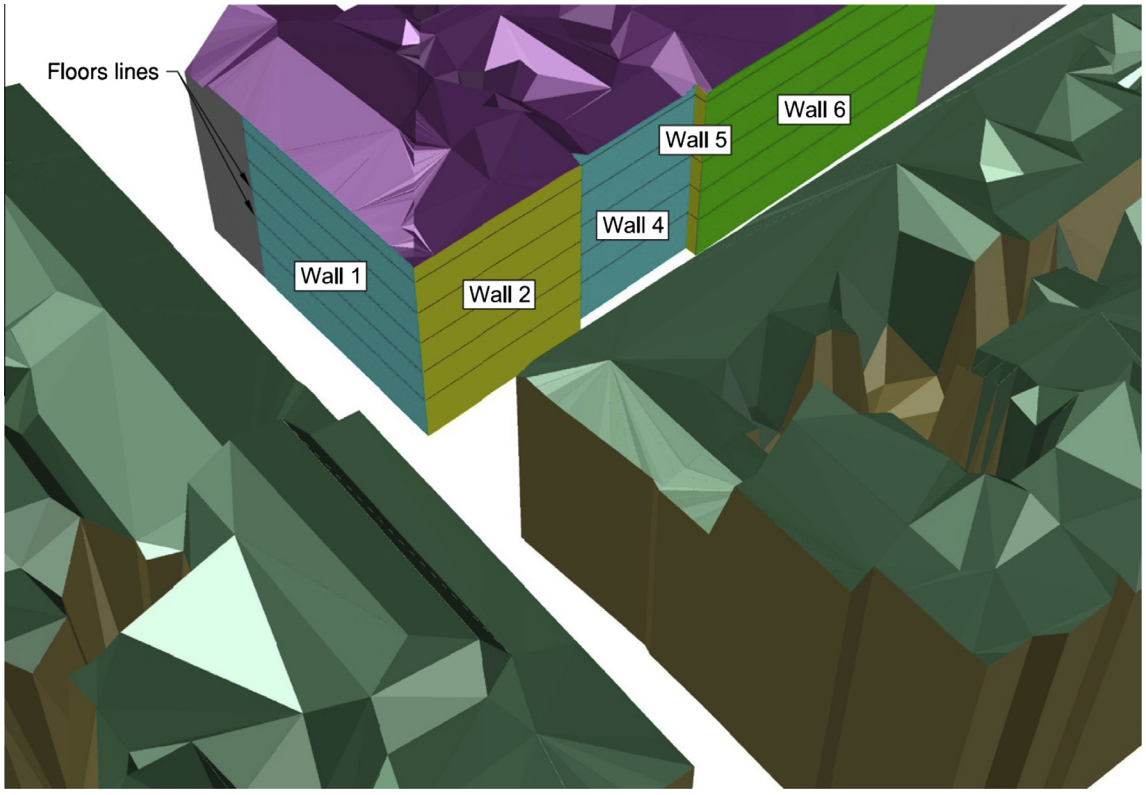

Fig. 10. The triangulation model obtained from LiDAR data (ii).

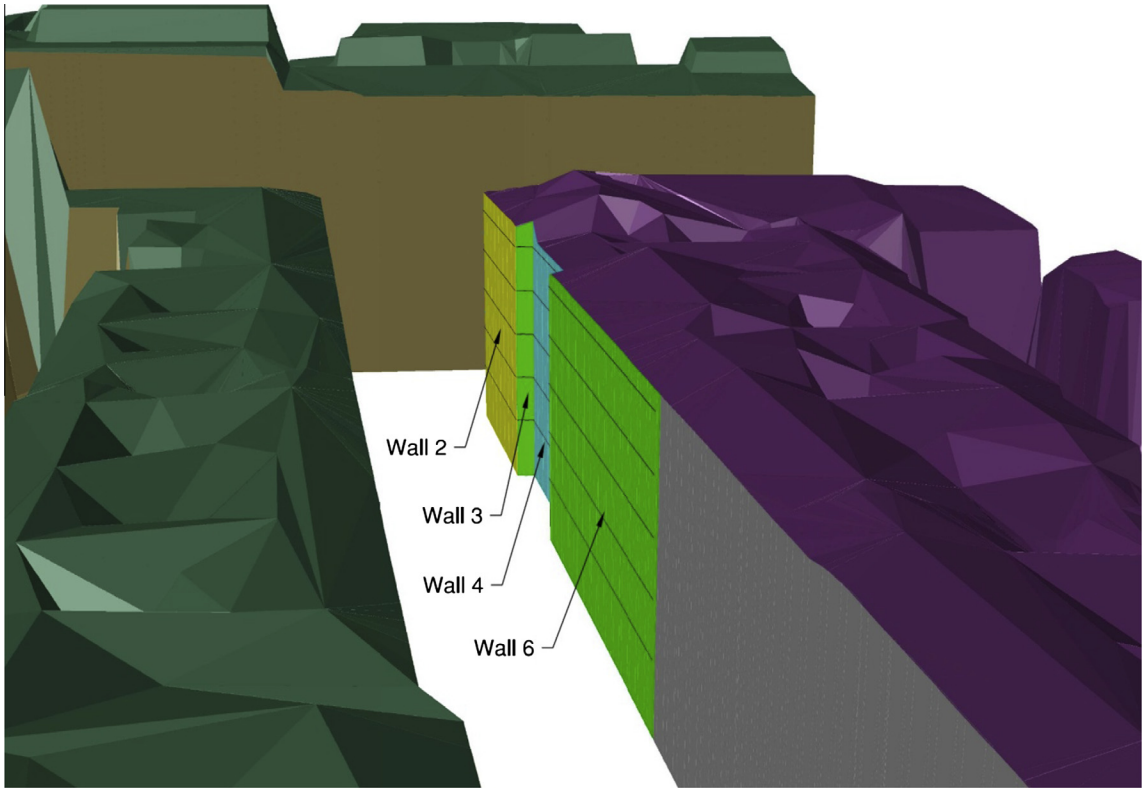

Fig. 11. The triangulation model obtained from LiDAR data (iii).

of BIPV products in Spain that was developed by Sanchez et al. [42]. He presents yearly results of solar photovoltaic elements that have been installed on the different facades of a particular building.

Finally, he compares the values of each wall with respect to the optimal plane. South facing walls presented about 66% with respect to the optimal plane, whereas eastern ones presented

Table 1
Number of points of testing for each wall and floor.

Ref wall	Surface (m^2)	Number of test-points				
		Ground floor	Floor 1	Floor 2	Floor 3	Floor 4
Wall 1	386	652	466	457	483	482
Wall 2	276	313	231	305	226	238
Wall 3	20	29	18	29	18	21
Wall 4	221	284	219	276	204	192
Wall 5	20	24	18	20	18	17
Wall 6	486	728	514	551	512	556

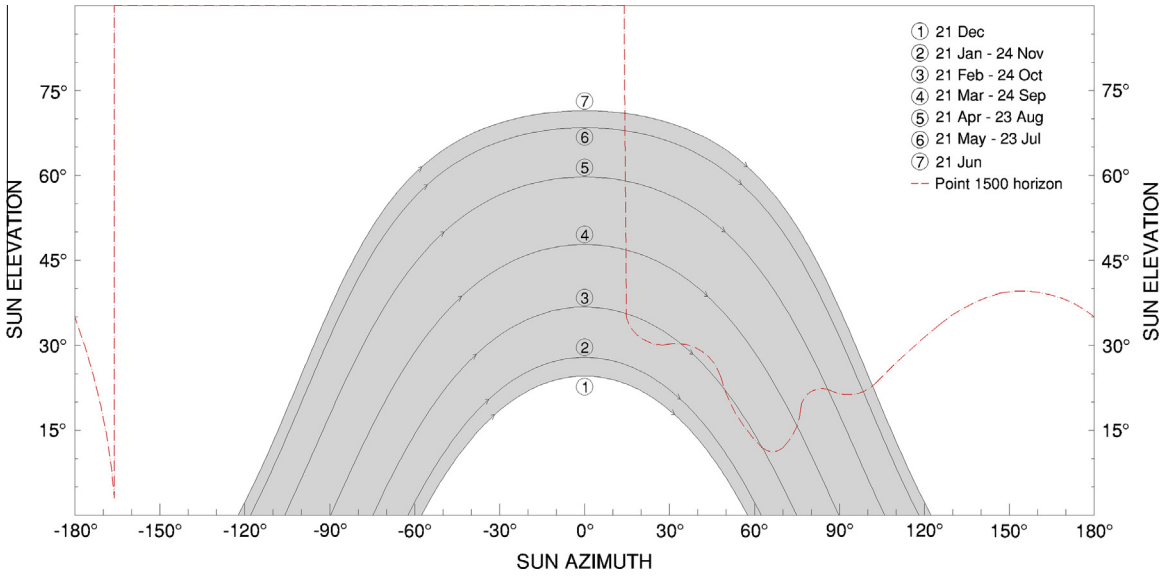

Fig. 12. Visible sky horizon for test-point 1500 (Wall 1).

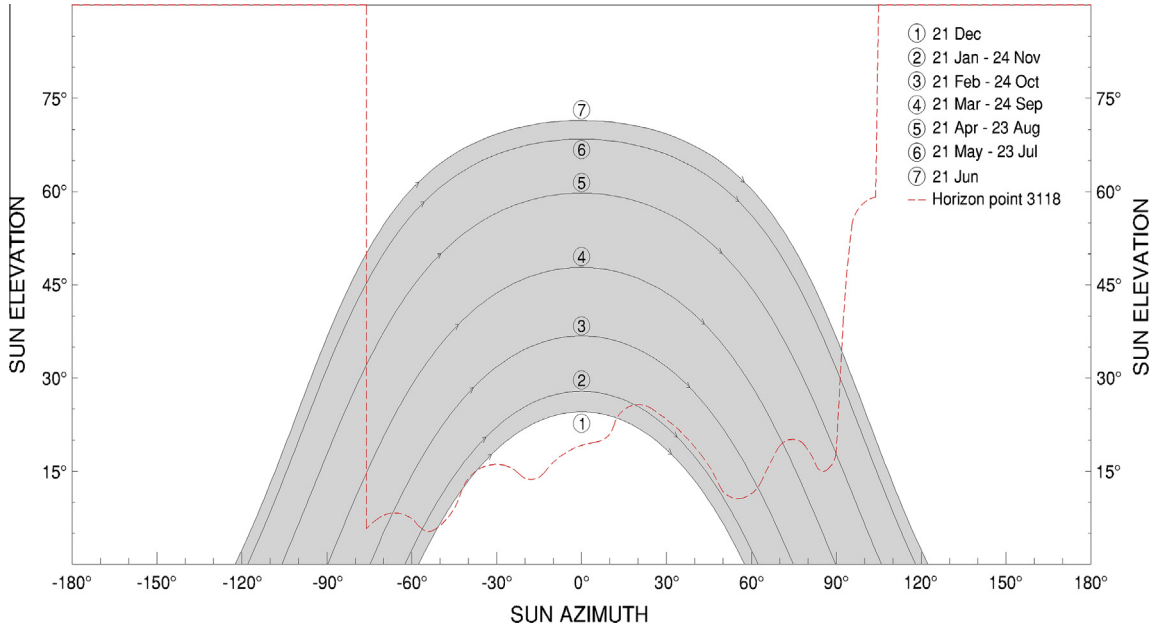

Fig. 13. Visible sky for test-point 3118 (Wall 2).

about 49% and western ones about 38%. The difference between eastern and western walls was explained by a nearby western mountain, whereas the other walls are free of shadows. So east and west oriented facades should present at around 49%.

In the case of Logroño, the optimal plane can harvest up to 1760 kW h/m^2 [39]. Walls that face southward show a maximum irradiance value of 1100 kW h/m^2 (wall number 2), which means about 62.5% with respect to the optimally-oriented plane. This is

lower than the percentage presented in [42] for a southward facade (66%), and it is due to a small disorientation of 11° with respect to the south and to the shading irradiance losses.

Wall number 1 is oriented westward and has an azimuth angle of 285°. Thus, the maximum value (600 kW h/m^2) is 34% with respect to the optimal angle, whereas wall number 3 is southeast-oriented, having a maximum value of 974 kW h/m^2, about 55% with respect to the optimal plane. The differences in these values when compared to [42] are logical if one considers that they are not perfectly oriented in the case of Logroño. So, in the case of southern influence, they present higher values, whereas a northern orientation reduces this percentage.

3. Results and discussion

3.1. 5-min analysis

As shown in Fig. 14, the 5-min profiles of each test-point for periods 5–8 of July clearly represent the scenario in which they are positioned. Fig. 14a shows the 5-min profiles of the global

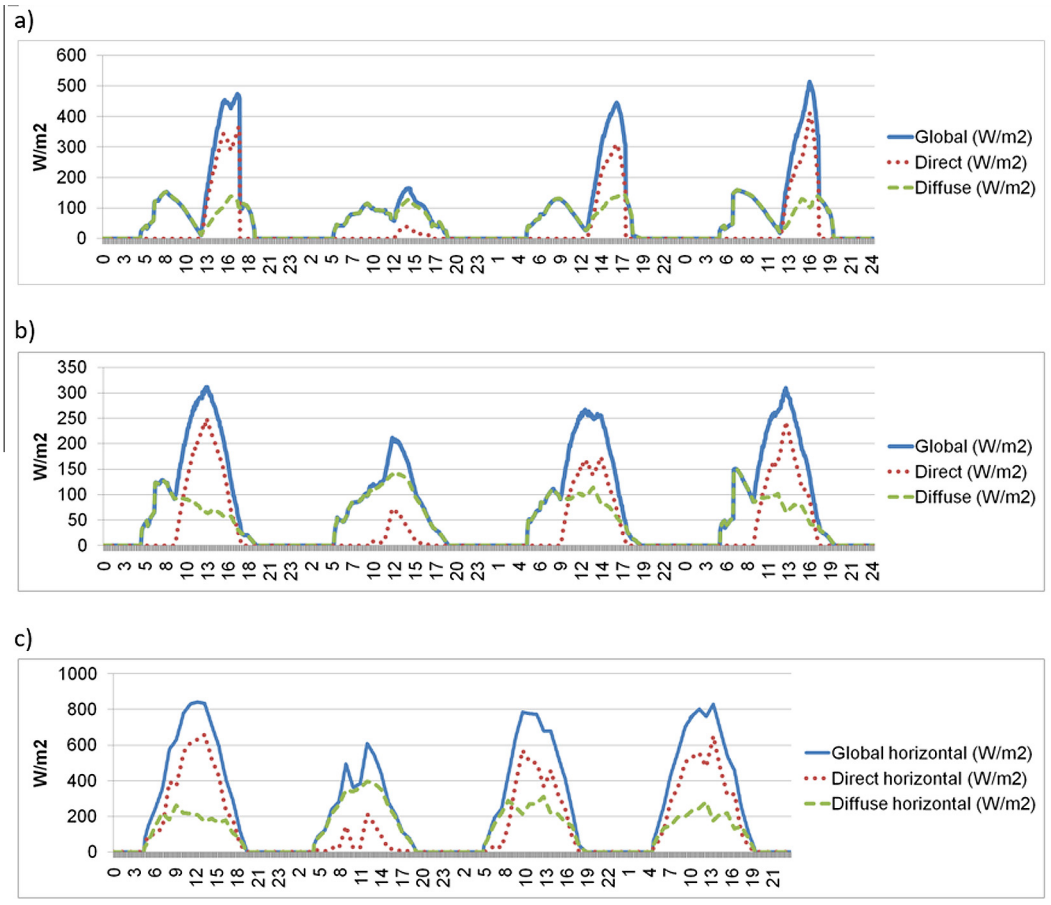

Fig. 14. Global, direct and diffuse irradiance terms for the July 5–8 period: (a) test-point 1500 (Wall 1); (b) test-point 3118 (Wall 2); (c) reference horizontal plane.

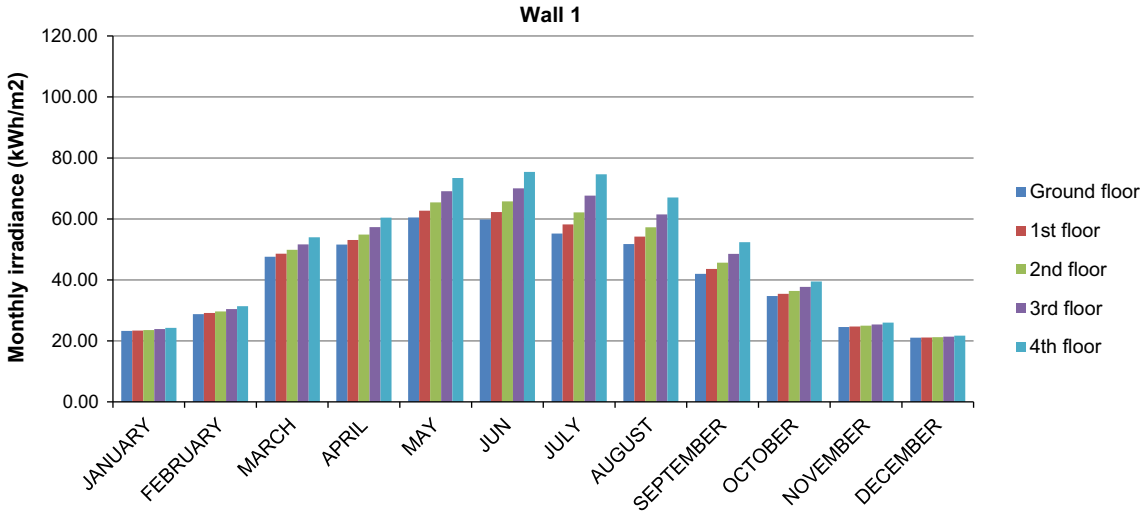

Fig. 15. Results of global irradiation of wall number 1.

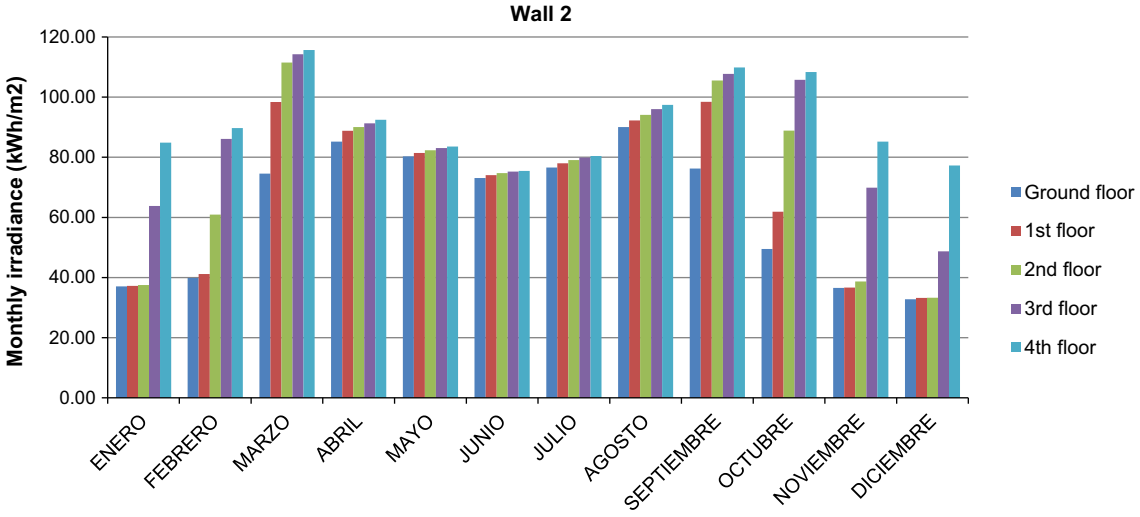

Fig. 16. Results of global irradiation of wall number 2.

Table 2
Annual global irradiance results (kW h/m^2).

GLOBAL IRRADIANCE (kW h/m^2)		Mean (kW h/m^2)	Maximum (kW h/m^2)	Minimum (kW h/m^2)	Standard deviation (kW h/m^2)
WALL No. 1	Ground floor	501	509	493	5
	Floor 1	517	525	510	5
	Floor 2	537	548	527	7
	Floor 3	565	578	549	9
	Floor 4	600	620	580	12
WALL No. 2	Ground floor	752	811	717	22
	Floor 1	822	867	786	20
	Floor 2	897	947	853	27
	Floor 3	1022	1087	949	44
	Floor 4	1100	1119	1065	42
WALL No. 3	Ground floor	731	761	704	14
	Floor 1	775	798	750	14
	Floor 2	826	864	790	19
	Floor 3	904	958	853	29
	Floor 4	974	1085	917	46
WALL No. 4	Ground floor	748	807	641	37
	Floor 1	817	875	666	44
	Floor 2	893	972	712	57
	Floor 3	1013	1093	737	73
	Floor 4	1064	1117	793	74
WALL No. 5	Ground floor	575	588	562	8
	Floor 1	602	613	592	7
	Floor 2	627	639	616	8
	Floor 3	653	667	638	9
	Floor 4	681	691	669	7
WALL No. 6	Ground floor	768	805	734	20
	Floor 1	840	872	805	20
	Floor 2	920	964	877	27
	Floor 3	1047	1098	977	39
	Floor 4	1105	1116	1082	37

(blue), direct (red) and diffuse (green) terms in test-point number 1500, which is located on the wall 1, facing the west. So, during the afternoon, the direct irradiance grows as the sun's elevation decreases. In the matter of diffuse irradiance, the effect of the nearby western building's reflected irradiance during morning hours must be noted.

In the case of a test-point facing south (Fig. 14b), the diffuse and direct irradiance terms affect all day long. The azimuth value of wall 2 (15° west), and the nearby southern building increase the diffuse irradiance term during the morning. Fig. 14c shows the profiles of the reference solar irradiance terms over a horizontal plane.

3.2. Monthly analysis

As previously indicated, the results are stored in a 5-min temporal basis. Thus, it is possible to group them and create monthly sums on which to observe the seasonal trend of every facade. Monthly results of the walls number 1 and 2 are discussed, since they are representative of the two main directions among the facades of the building.

Fig. 15 shows the monthly values of solar irradiation per month and floor of wall number 1. It can clearly be seen that, from March onwards, the increasing direct irradiation causes greater

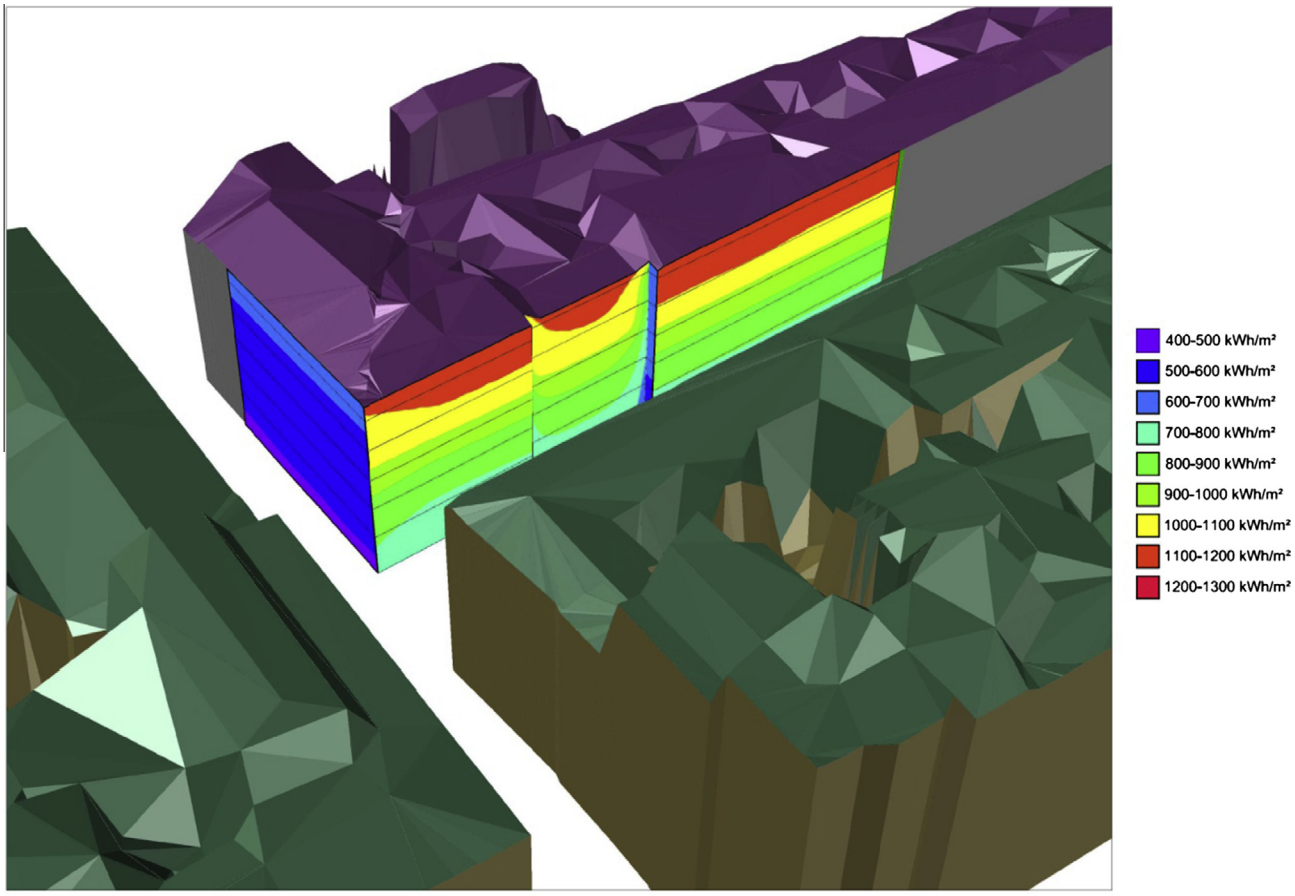

Fig. 17. Annual results of global irradiation on facades (i).

differences in captured irradiation between different floors. January, November and December present a little influence from direct irradiance. Thus, they limit the collected irradiance to the diffuse portion. The main reason for this phenomenon is the northwest orientation of the facade, which is combined with the effect of the adjacent building situated to the west.

Monthly irradiance values of wall number 2 are much higher than in the wall number 1. As it can be seen in Fig. 16, during the winter period the lower floors are not exposed to direct sunlight, whereas those located on the top of the building are clearly affected by this type of irradiance. Such high values of irradiance in the winter months, which are comparable to those in summer and even higher, are due to the solar geometry presented in those periods. During winter months, the Sun's elevation is not so high, and lower values of angle of incidence between the sun rays and the facades allow to achieve an optimal irradiance harvesting.

March and September (equinox months) are of great importance, as they are the months in which the captured solar irradiation reaches its maximum on upper floors. The maximization of the uptake of solar irradiance during these months is due to both, the number of hours of sunshine in March and September and the angle of incidence values. Due to the geometric factor reduction, even if the maximum solar irradiance is produced between the months April and August, the direct irradiance acting over the wall number 2 is significantly decreased. As a consequence, the global irradiation over that face of the building's envelope is lower.

In the case of the ground floor, the maximum occurs during the months of April and August, considerable different from the upper floors. Although this phenomenon was previously explained, in this case it is also related to another factor: the conditioning effect of the nearby southern building.

3.3. Annual analysis

The analysis of annual irradiation that influences the different facades that are considered for the model application shows great variability in relation to orientation and height from the ground.

Global irradiance results (mean, maximum, minimum and standard deviation) are presented by facade and floor level on Table 2. It should be remembered that while walls number 2, 4 and 6 are the most favorable in terms of irradiance incidence, as they are practically southward-oriented, walls number 1 and 5 present the least favorable cases with a westward orientation (see Fig. 8).

In general, a major elevation of the points implies a major incidence of solar irradiation. This is rather logical if one considers the produced shade by nearby buildings. In addition, the values of standard deviation become larger as the height of the points increases. However, there are some peculiarities that are described below.

Wall number 1 is a perfect example of a facade that receives little irradiation throughout the year, as shown in Figs. 17 and 18. The ground floor has an average irradiance value of 501 kW h/m^2 and the highest floor has an average of 600 kW h/m^2, which means that there is a difference between them of less than a 20%.

The study of wall number 5 (Fig. 18), which presents the same orientation as wall number 1, shows greater values of irradiation, while it maintains the difference of 20% between the lower and upper zones. This effect is explained by the influence of the western building, which is higher than in the case of the wall number 5,

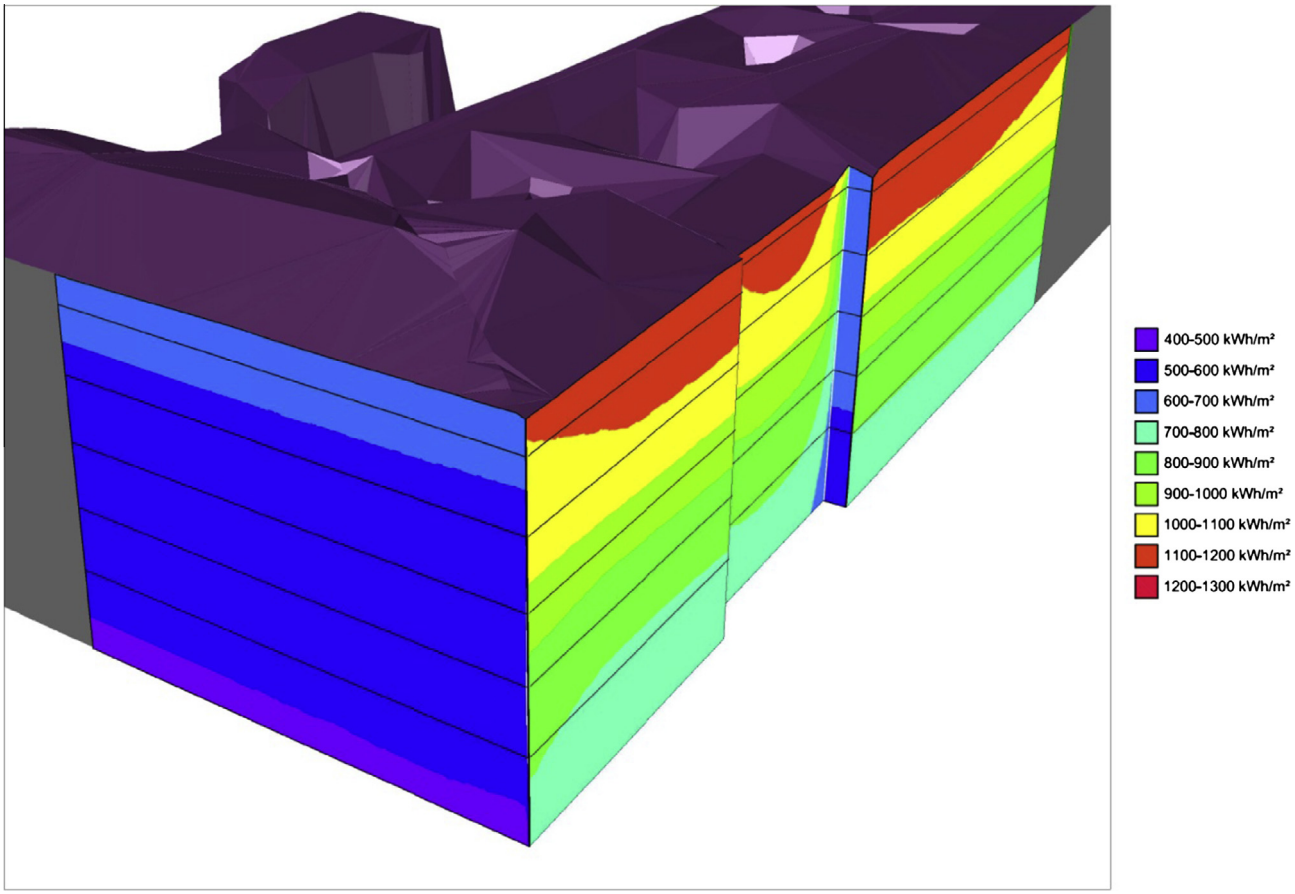

Fig. 18. Annual global irradiation on facades results (ii).

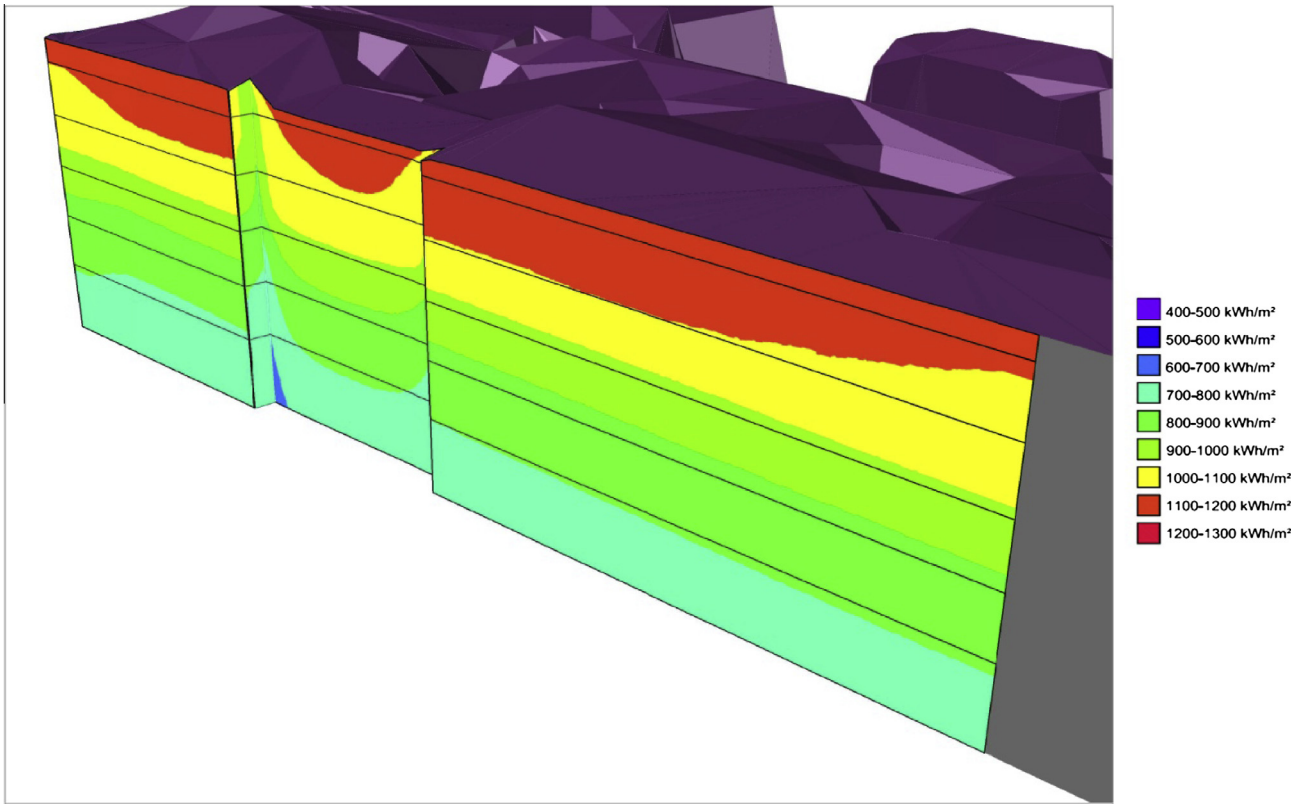

Fig. 19. Annual results of global irradiation on facades (iii).

which is not just affected by wall 1. In contrast, the influence of the nearby southern building is almost irrelevant because of the wall orientation.

Analyzing those walls that are equally oriented (numbers 2, 4 and 6), a lower irradiation level is observed on wall number 4. It is due to the effect of shading produced by walls number 3 and 5. Walls number 2 and 6 receive a similar irradiation level, although it is always lower in the case of wall number 2, since it is closer to the nearby western building, which is higher than southern building.

The analysis of wall number 2 reveals two remarkable points. The first is that the gain between the upper and the lower floors is about 46%, with 752 kW h/m^2 on the ground floor and 1100 kW h/m^2 on the 4th floor. The other important point is that the irradiance values of the third and fourth floors reach values that exceed 1000 kW h/m^2. These values of irradiation could be converted to 800 kW h/kWp of photovoltaic efficiency, assuming an 80% performance ratio. An efficiency value of 800 kW h/kWp is considered to be low, but regarding the progressive and continued reduction in costs of photovoltaic products, it could be economically feasible in the near future. It is noteworthy that in certain areas of northern Europe (e.g., the City of Copenhagen in Denmark), where the commitment to renewable energy generation is worldwide known, there are efficiency values of 990 kW h/kWp for optimally-oriented planes [39].

The analysis of wall number 6 is similar to the one presented for number 2, since they are equality oriented. The values of gain of irradiation between top and bottom floors are about 44%, having sufficiently high irradiance levels in certain areas to make it interesting to locate photovoltaic elements over the building's envelope (above 1000 kW h/m^2).

In the case of the wall number 4, as we get a farther perspective from the areas of transition of facades, irradiation increases to values that are similar to those found in walls 2 and 6, reaching irradiation values that exceed 1000 kW h/m^2.

Finally, it can be seen on Table 2 and in Fig. 19 that wall number 3 shows average irradiation values greater than those presented by its parallel walls number 1 and 5. This is mainly due to the orientation, because walls number 1 and 5 are northwest-oriented, whereas wall number 3 faces southeast with an azimuth value of 105°.

4. Conclusions

Proper use of building facades for photovoltaic energy production could provide 100% of the energy requirements of households in cities. A previous analysis of building envelopes' photovoltaic potential is essential to design energy-efficient and environmentally sustainable cities.

The proposed method enables one to estimate the solar irradiance (kW h/m^2) and to visualize it in every area of each facade of a city by the use of LiDAR information and monthly irradiance data. Results are stored on a 5-min basis so it is possible to perform monthly or yearly analyses. The influence of the building's own shading and the one produced by nearby buildings is one of the main effects of an increasing irradiation gradient as the upper points are analyzed. However, the orientation of the facades has been proven to be the most important influencing parameter to obtain a higher irradiation value. Monthly analyses demonstrate that the best-oriented facades have the greatest irradiance harvesting during equinox months.

The algorithm has been validated on different building envelopes distributed around various geographical areas. Therefore, it can be stated that it is perfectly extrapolated to any city where LiDAR and solar irradiance information are available. Thus, the solar irradiance over the buildings' envelopes can be rigorously analyzed, allowing to select the solution that best meets the trinomial performance/production/profitability in each building.

This algorithm succeeds in obtaining a map of solar radiation captured by the envelope of any urban building (0.5 m grid resolution) using a new methodology that estimates the photovoltaic power generation based on the geographic location and influence of shading caused by adjacent buildings.

Arranging a solar irradiation map of the buildings of a city is a valuable tool for sustainable urban planning with non-carbonized criteria in important applications. Such applications may include: (1) an analysis of energy efficiency of the building, (2) selection of materials for the building envelope and insulation according to the irradiation received in each point of the facade, (3) profitability monitoring of the photovoltaic installation depending on its irradiance zone, (4) adapting the esthetics of existing buildings according to their irradiation (less monotonous facades), (5) buildings restoration to improve the energy efficiency and the electric generation, (6) refurbishing and regenerating degraded urban areas or (7) planning new sustainable energy developments.

References

[1] European Commission (Brussels), Europe 2020. A strategy for smart, sustainable and inclusive growth; 2010.
[2] Jelle BP. Traditional, state-of-art and future thermal building insulation materials and solutions-properties, requirements and possibilities. Energy Build 2011;43:2549–63.
[3] Jelle BP, Breivik C, Røkenes HD. Building integrated photovoltaic products: a state-of-the-art review and future research opportunities. Sol Energy Mater Sol Cells 2012;100:69–96.
[4] Cerón I, Caamaño-Martín E, Neila FJ. State-of-the-art' of building integrated photovoltaic products. Renew Energy 2013;58:127–33.
[5] Hsieh Chun-Ming, Chen Yi-An, Tan Hongwei, Lo Pei-Fang. Potential for installing photovoltaic systems on vertical and horizontal building surfaces in urban areas. Sol Energy 2013;93:312–21.
[6] Ropp ME, Begovic M, Rohatgi A, Long R. Design considerations for large roof-integrated photovoltaic arrays. Prog Photovoltaics Res Appl 1997;5:1302–15.
[7] Esclapés J, Ferreiro I, Piera J, Teller J. A method to evaluate the adaptability of photovoltaic energy on urban façades. Sol Energy 2014;105:414–27.
[8] Zogou O, Stapountzis H. Energy analysis of an improved concept of integrated PV panels in an office building in central Greece. Appl Energy 2011;88:853–66.
[9] Sun Liangliang, Lin Lu, Yang Hongxing. Optimum design of shading-type building-integrated photovoltaic claddings with different surface azimuth angles. Appl Energy 2012;90:233–40.
[10] Mandalaki M, Zervas K, Tsoutsos T, Vazakas A. Assessment of fixed shading devices with integrated PV for efficient energy use. Sol Energy 2012;86:2561–75.
[11] Chae YT, Kim J, Park H, Shin B. Building energy performance evaluation of building integrated photovoltaic (BIPV) window with semi-transparent solar cells. Appl Energy 2014;129:217–27.
[12] James PAB, Jentsch MF, Bahaj AS. Quantifying the added value of BIPV as a shading solution in atria. Sol Energy 2009;83:220–31.
[13] Kanga Seokyoun, Hwang Taeyon, Kim Jeong Tai. Theoretical analysis of the blinds integrated photovoltaic modules. Energy Build 2012;46:86–91.
[14] Prasad DK, Snow M. Examples of successful architectural integration of PV: Australia. Prog Photovoltaics Res Appl 2004;12:477–83.
[15] Yoo Seung-Ho, Lee Eun-Tack, Lee Jong-Keuk. Building integrated photovoltaics: a Korean case study. Sol Energy 1998;64:151–61.
[16] Pagliaro M, Ciriminna R, Palmisano G. BIPV: merging the photovoltaic with the construction industry. Prog Photovoltaics Res Appl 2010;18:61–72.
[17] Paul D, Mandal SN, Mukherjee D, Bhadra SR. Optimization of significant insolation distribution parameters – a new approach towards BIPV system design. Renew Energy 2010;35:2182–91.
[18] Pérez M, Fthenakis V, Kim H, Pereira AO. Façade-integrated photovoltaics: a life cycle and performance assessment case study. Prog Photovoltaics Res Appl 2012;20:975–90.
[19] Súri M, Huld TA, Dunlop ED, Ossenbrink HA. Potential of solar electricity generation in the European Union member states and candidate countries. Sol Energy 2007;81:1295–305.
[20] Huld T, Müller R, Gambardella A. A new solar radiation database for estimating PV performance in Europe and Africa. Sol Energy 2012;86:1803–15.
[21] Salazar JH. Calculation of the shadow-penumbra relation and its application on efficient architectural design. Sol Energy 2014;110:139–50.
[22] Ioannou AK, Stefanakis NE, Boudouvis AG. Design optimization of residential grid-connected photovoltaics on rooftops. Energy Build 2014;76:588–96.
[23] Mulcué-Nieto LM, Mora-López L. Methodology to establish the permitted maximum losses due to shading and orientation in photovoltaic applications in buildings. Appl Energy 2015;137:37–45.

[24] Martinez-Rubio A, Sanz-Adan F, Santamaría J. Optimal design of photovoltaic energy collectors with mutual shading for pre-existing building roofs. Renew Energy 2015;78:666–78.
[25] Melo EG, Almeida MP, Zilles R, Grimoni JA. Using a shading matrix to estimate the shading factor and the irradiation in a three-dimensional model of a receiving surface in an urban environment. Sol Energy 2013;92:15–25.
[26] Redweik P, Catita C, Brito M. Solar energy potential on roofs and façades in an urban landscape. Sol Energy 2013;97:332–41.
[27] Santamaria J, Sanz-Adan F, Martinez-Rubio A, Valbuena M. Use of LiDAR technology for detecting energy efficient roofs in urban areas. DyNA Spain 2015;90:636–42.
[28] Catita C, Redweik P, Pereira J, Brito MC. Extending solar potential analysis in buildings to vertical façades. Comput Geosci 2014;66:1–12.
[29] Zhou Q, Newmann U. 2.5 dual contouring: a robust approach to creating building models from Aerial LiDAR point clouds. Computer Vision-ECCV 2010;1:115–28. Available from: <http://link.springer.com/chapter/10.1007%2F978-3-642-15558-1_9>.
[30] Zhou Q, Neumann U. Modeling residential urban areas from dense aerial LiDAR point clouds. Lect Notes Comput Sci 2012;7633:91–8.
[31] Truong-Hong L, Laefer DF. Octree-based, automatic building façade generation from LiDAR data. Comput Aided Des 2014;53:46–61.
[32] Vardimon R. Assessment of the potential for distributed photovoltaic electricity. Renew Energy 2011;36:591–4.
[33] Zomer C, Nobre A, Cassatella P, Reindl T, Rüther R. The balance between aesthetics and performance in building-integrated photovoltaics in the tropics. Prog Photovoltaics Res Appl 2014;22:744–56.
[34] Gooding J, Crook R, Tomlin AS. Modelling of roof geometries from low-resolution LiDAR data for city-scale solar energy applications using a neighbouring buildings method. Appl Energy 2015;148:93–104.
[35] Tooke TR, Van der Laan M, Coops NC. Mapping demand for residential building thermal energy services using airborne LiDAR. Appl Energy 2014;127:125–34.
[36] Cooper PI. The absorption of radiation in solar stills. Sol Energy 1969;12:333–46.
[37] Perez R, Seals R, Ineichen P, Stewart P, Menicucci D. A new simplified version of the Perez diffuse irradiance model for tilted surfaces. Sol Energy 1987;39:221–31.
[38] Plan Nacional OrtofotogrametríaAérea PNOA. Spanish Government. <http://pnoa.ign.es/>.
[39] Institute for Energy, Renewable Energy Unit. DB solar radiation of PVGIS. European Commission, Joint Research Centre; 2016. Available from: <http://re.jrc.ec.europa.eu/pvgis>.
[40] Graham V, Hollands K. A method to generate synthetic hourly solar radiation globally. Sol Energy 1990;44(6):333–41.
[41] Aguiar R, Collares-Pereira. TAG: a time-dependent auto-regressive, Gaussian model. Sol Energy 1992;49(3):167–74.
[42] Sanchez E, Izard J. Performance of photovoltaics in non-optimal orientations: an experimental study. Energy Build 2015;87:211–9.